New Journal of Physics
The open access journal at the forefront of physics

Deutsche Physikalische Gesellschaft DPG IOP Institute of Physics

PAPER • OPEN ACCESS

Open circuit voltage generated by dragging superconducting vortices with a dynamic pinning potential

To cite this article: Cun Xue *et al* 2019 *New J. Phys.* **21** 113044

New Journal of Physics
The open access journal at the forefront of physics

Deutsche Physikalische Gesellschaft DPG
IOP Institute of Physics

Published in partnership with: Deutsche Physikalische Gesellschaft and the Institute of Physics

OPEN ACCESS

RECEIVED
29 August 2019

REVISED
23 October 2019

ACCEPTED FOR PUBLICATION
5 November 2019

PUBLISHED
25 November 2019

PAPER

Open circuit voltage generated by dragging superconducting vortices with a dynamic pinning potential

Cun Xue[1], An He[2], Milorad V Milošević[3], Alejandro V Silhanek[4] and You-He Zhou[5,6]

[1] School of Mechanics, Civil Engineering and Architecture, and MIIT Key Laboratory of Dynamics and Control of Complex Systems, Northwestern Polytechnical University, Xi'an 710072, People's Republic of China
[2] College of Science, Chang'an University, Xi'an 710064, Peoples Republic of China
[3] Departement Fysica, Universiteit Antwerpen, Groenenborgerlaan 171, B-2020 Antwerpen, Belgium
[4] Experimental Physics of Nanostructured Materials, Q-MAT, CESAM, Université de Liège, B-4000 Sart Tilman, Belgium
[5] Key Laboratory of Mechanics on Disaster and Environment in Western China attached to the Ministry of Education of China, and Department of Mechanics and Engineering Sciences, Lanzhou University, Lanzhou 730000, People's Republic of China
[6] School of Aeronautics, Northwestern Polytechnical University, Xi'an 710072, People's Republic of China

E-mail: xuecun@nwpu.edu.cn

Keywords: time-dependent Ginzburg–Landau, dynamic vortex pinning, mesoscopic superconducting dynamo

Supplementary material for this article is available online

Abstract

We theoretically investigate, through Ginzburg–Landau simulations, the possibility to induce an open circuit voltage in absence of applied current, by dragging superconducting vortices with a dynamic pinning array as for instance that created by a nearby sliding vortex lattice or moving laser spots. Different dynamic regimes, such as synchronous vortex motion or dynamic vortex chains consisting of laggard vortices, can be observed by varying the velocity of the sliding pinning potential and the applied magnetic field. Additionally, due to the edge barrier, significantly different induced voltage is found depending on whether the vortices are dragged along the superconducting strip or perpendicular to the lateral edges. The output voltage in the proposed mesoscopic superconducting dynamo can be tuned by varying size, density and directions of the sliding pinning potential.

1. Introduction

In an irradiated conductor, the momentum of the incident electromagnetic wave is absorbed by free carriers and consequently, the electron system can acquire a translational motion that manifest itself in the form of a current or a voltage. This phenomenon, known as the photon-drag effect, was extensively studied first by Grinberg [1] and later on by Gibson and co-workers [2–4]. Similarly, an electromotive force can be induced in a current-free type-II superconductor in the mixed state by dragging the induced vortices (carriers of units of magnetic flux quanta) [5, 6]. This has been experimentally demonstrated by pulling a vortex lattice by another vortex lattice spatially separated from the former, but magnetically coupled to it [7]. An analogous outcome can be expected by dragging the vortex lattice with a sliding potential as the one created by an inhomogeneous magnetic field. This approach has been recently proposed by Bumby *et al* [8] to generate an open-circuit voltage from a high-T_c superconducting dynamo. A similar coupling has been explored in other bi-layer systems, such as the coupling between vortex lattice and an electron gas in superconductor-semiconductor hybrids [9], the Coulomb interaction in two coupled electronic layers (electron-drag effect) [10, 11], and the interplay between the vortex lattices and corotating optical lattices [12]. Recently, a somewhat related physics concerning coupled one-dimensional channels of particles with Yukawa interactions has been theoretically addressed in [13]. In this case, a transition from locked flow, where particles in both the driving and the dragged channels move together, to decoupled flow, where the particles in the undriven channel move at a lower velocity than the particles in the driven channel, has been reported. A coupling–decoupling transition can also be observed for individually dragged particles in systems with quenched disorder [14].

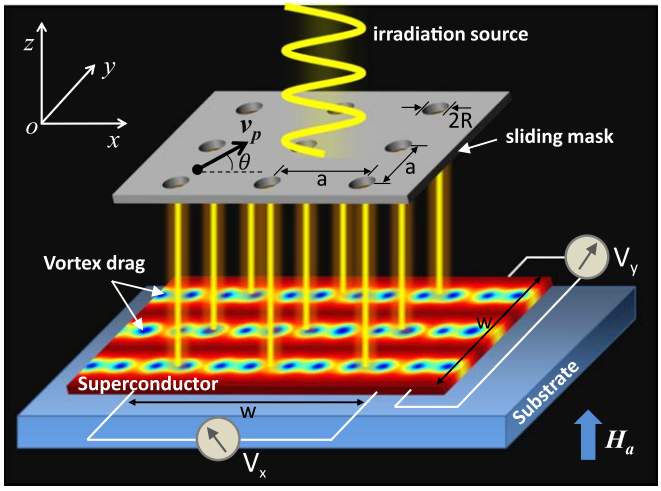

Figure 1. Schematic representation of a possible realization of a sliding pinning potential able to drag vortices in a superconducting strip without applied current. Besides its strength, the dynamic pinning potential can be tuned by varying the velocity v_p and in-plane orientation θ of its motion. The superconducting strip of width w (y direction) and infinite length (x direction) is exposed to a perpendicular magnetic field H_a. The induced voltage drops V_x and V_y are calculated between the points as indicated in the figure. The considered pinning landscape comprises a square array (with period a) of circular pinning sites (with radius R).

From an experimental standpoint, new approaches have been developed to manipulate individual vortices by using the magnetic force caused by a magnetic tip [15–17] or a tiny electromagnet [18, 19]. Kermen *et al* showed that the local mechanical stress can also be used to manipulate individual vortices [20]. Additionally, Veshchunov *et al* introduced a focused laser beam to realize a fast and precise manipulation of individual vortices [21], in the same way as with optical tweezers. A similar local heating of the superconductor has also been realized by a tunneling current through a local probe [22].

In the present work, we investigate the open circuit voltage as a consequence of vortex dragging by the sliding pinning potential, by means of time-dependent Ginzburg–Landau (tdGL) equations. The driving potential landscape can stem from, e.g. an array of magnetic dots [23, 24], dynamic spatially periodic light excitation (as schematically shown in figure 1), shifting traps as those successfully used to manipulate colloidal particles [25–31], or skyrmions in an adjacent layer [32].

Unlike previously investigated spatially confined and time-varying pinning potential [33, 34], the dynamic pinning discussed here changes both in space and time. We demonstrate that the induced voltage strongly depends on whether the vortex lattice is dragged parallel or perpendicular to the borders of a superconducting strip. Additionally, the open circuit voltage can be tuned by adjusting the size and density of traps within the sliding pinning potential.

2. Model system and theoretical formalism

For the model system, as shown in figure 1, we consider a superconducting strip of width w and infinite length along the x-axis. The sample contains no intrinsic random pinning, bears no electric current and is exposed to a perpendicular magnetic field H_a. A square array of external perturbations acting as pinning potential slides over the superconducting strip with a velocity $\mathbf{v}_p$. The size, density and motion of the sliding pinning potential are tunable by varying radius R, period a and sliding orientation given by the angle θ with respect to the x-axis. As depicted in figure 1, the induced voltage output V_x and V_y are measured between two points along the superconducting strip and perpendicular to it, respectively.

In order to study the vortex dynamics and the resulting induced voltage in such a superconducting strip with a dynamic pinning landscape, we employed the generalized tdGL equations, which were widely used to analyze the vortex dynamics, current-voltage characteristics and magnetoresistance [33, 35, 36]:

$$\frac{u}{\sqrt{1+\gamma^2|\psi|^2}}\left(\frac{\partial}{\partial t}+\frac{\gamma^2}{2}\frac{\partial|\psi|^2}{\partial t}\right)\psi=(\nabla-\mathrm{i}\mathbf{A})^2\psi+(f(t,\mathbf{r})-|\psi|^2)\psi, \tag{1}$$

$$\frac{\partial\mathbf{A}}{\partial t}=\mathrm{Re}\left[\psi^*(-\mathrm{i}\nabla-\mathbf{A})\psi\right]-\kappa^2\nabla\times\nabla\times\mathbf{A}. \tag{2}$$

In these equations, the distances are scaled by the coherence length ξ at the working temperature T, the order parameter ψ by its equilibrium value in the absence of magnetic field, the vector potential $\mathbf{A}$ by $\Phi_0/2\pi\xi(T)$, the

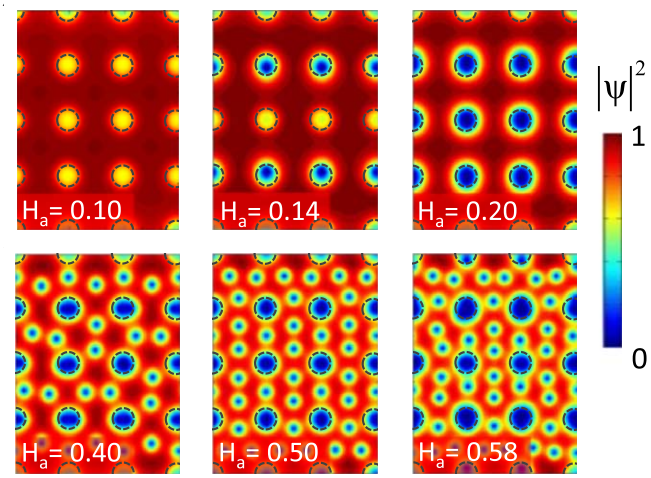

Figure 2. Snapshots of the Cooper-pair density distributions in the sample, showing vortex states in presence of a static pinning potential ($v_p = 0$) at magnetic fields $H_a = 0.1, 0.14, 0.2, 0.4, 0.5, 0.58$. The length of simulated area is $L = 24.4$ and the strip extends periodically along the horizontal direction. The radius and the period of the pinning potential (indicated with a dash black line) are $R = 1.63$ and $a = 8.13$, respectively.

time by the Ginzburg–Landau relaxation time, $\tau_{\rm GL} = \pi\hbar/8k_B(T_c - T)u$ and the magnetic field H_a by $H_{c2} = \Phi_0/2\pi\xi^2$. The voltage in units of φ_0 can be calculated by $\int \frac{\partial \mathbf{A}}{\partial t} \mathrm{d}\mathbf{l}$ in the direction of interest. The parameter $u = 5.79$ is a suitable value for most low-T_c superconductors according to the microscopic theory [35, 37]. Parameter γ accounts for inelastic scattering (dirtiness) of the superconducting film, and we take a reasonable value $\gamma = 20$ for the considered sample [38, 39]. The function $f(t, \mathbf{r})$ describes the dynamic pinning potential in the superconducting strip, with $f = 0$ in the perturbed region and $f = 1$ in the unperturbed region of the sample. Although the model of the pinning array is simplified, it can well catch the dragging effects of the dynamic pinning sites on the vortices. To model the unbounded strip along the x-axis, periodic boundary conditions are used in this direction, i.e. $\psi(x, y) = \psi(x + L, y)$ and $\mathbf{A}(x, y) = \mathbf{A}(x + L, y)$ where L is the length of the simulated part of the strip and it varies in the cases of pinning sites with different densities. The superconductor-vacuum boundary conditions $(\nabla - \mathrm{i}\mathbf{A})\psi|_n = 0$ are used in y directions. In what follows, we adopt $\xi = 73.8$ nm, $\kappa = 4$ and $w = 2.4$ μm in our simulations [39, 40]. For comparison, typical Nb thin films have $\xi(0) = 10$ nm and $\kappa = 15$ [41], for Al films it has been previously reported $\xi(0) = 90$ nm and $\kappa \sim 2$ [42], whereas for Pb, $\xi(0) = 34$ nm and $\kappa \sim 2$ [43]. Since the effective penetration depth is dependent on the thickness of the superconducting film, it can be varied in a large range of values without significantly altering T_c or ξ. In other words, the chosen values for the parameters used in our simulations are somewhat closer to those reported for Al films. Notice that the source of the pinning lattice is considered to be much larger laterally than the superconductor.

3. Results and discussions

Figure 2 shows different vortex configurations obtained at various magnetic fields when the pinning potential is static, which are very similar to the vortex states in presence of the conventional permanent artificial pinning sites extensively studied in the literature [44]. In what follows, the dynamic pinning potential starts sliding from these initial states at various magnetic fields. For the Meissner state ($H_a = 0.1$), the first panel in figure 2 shows that the superconducting condensate is only partially suppressed by the pinning potential. Interstitial vortices appear after each pinning site has been occupied by two vortices. The vortex cores are not necessarily located exactly in the center of the pinning potential due to the Lorentz force produced by the screening current flowing at the sample edges.

3.1. Vortex drag along the superconducting strip

Let us first discuss the case of dragging vortices along the x-axis by the dynamic pinning potential, i.e. the case $\theta = 0°$. As the vortices always move without crossing the sample lateral edges, there is no edge barrier to affect the vortex motion. In this case, V_x is zero and only V_y can be measured. As shown in figure 3(a), the voltage V_y at $H_a = 0.1$ is zero since there are no vortices inside the sample (Meissner state). For higher magnetic fields, a non-monotonic velocity dependence of the induced voltage is observed. For instance, the variations of V_y at $H_a = 0.14$ can be divided into two regions with increasing v_p (background with different colors). For slow pinning potential, V_y is proportional to v_p. In this case, the viscous force is weaker than the driving force

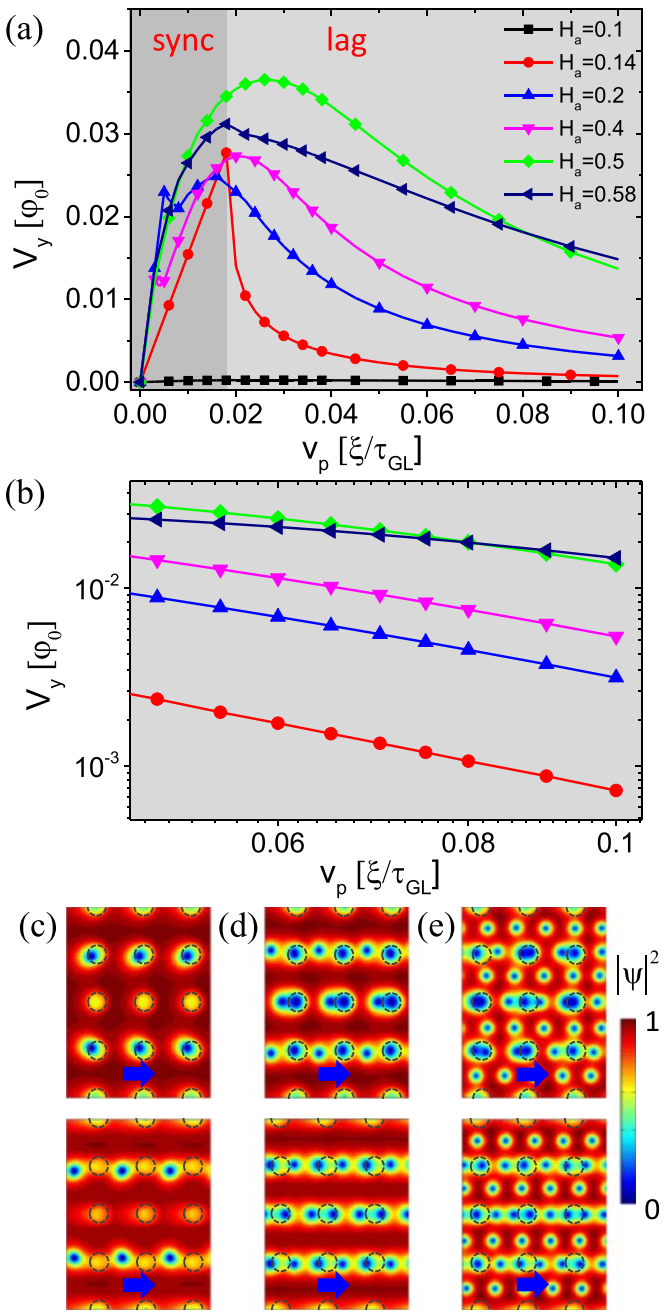

Figure 3. (a) The induced voltage (V_y) as a function of the velocity of the dynamic pinning potential (v_p) along the strip ($\theta = 0°$) at different magnetic fields. The parameters of the dynamic pinnings are $R = 1.63$ and $a = 8.13$. (b) Log–log plot of the high-velocity data shown in panel (a). The symbols respect the field labels in panel (a). (c)–(e) The upper (lower) panels represent the snapshots of Cooper pair density for the sliding pinning potential velocity $v_p = 0.014$ (0.06) at magnetic fields $H_a = 0.14$ (c), 0.2 (d), and 0.4 (e). Black dotted circles and blue arrows indicate the position of the sliding dynamic pinnings and the dragging direction in each snapshot. The strip is along horizontal direction. The time evolutions of the induced voltage $V_y(t)$ and the animated data of the dynamic vortex states can be seen in supplemental figures and movies is available online at stacks.iop.org/NJP/21/113044/mmedia (see footnotes 7 and 8).

produced by the sliding pinning potential, and consequently, a synchronous motion of the vortex lattice with the dynamic pinning potential is observed (see upper panel of figure 3(c)). With increasing velocity, however, the driving force exerted by the sliding pinning potential can no longer fully overcome the viscous force acting on the vortex lattice. Under these circumstances, a laggard (slippery) vortex motion is observed (see lower panel of figure 3(c)). This higher-speed regime seems difficult to access experimentally since in the present case it requires velocities $v_p \sim 0.1\xi/\tau_{GL} \sim 1$ km s^{-1}. However, this threshold velocity can be tuned by weakening the pinning strength (characterized by $f(t, \mathbf{r})$ in our calculations, see equation (1)). The log–log plot of figure 3(b) indicates that the induced voltage V_y decreases following a power-law dependence at higher velocity of the dynamic pinning potential. Similar dependence of the induced voltage as a function of sliding potential velocity has been

observed experimentally in the dc flux transformer introduced by Giaever [5, 6] and it has been discussed theoretically by Ekin *et al* [7].

With increasing magnetic field, a higher increasing rate of V_y is observed at low velocity as shown in figure 3(a). This is due to the motion of more vortices and because each pinning potential can trap a giant vortex and drag it synchronously (see supplemental figures[7]). The nonlinear increase of V_y observed in figure 3(a) at higher fields is due to the fact that laggard vortices coexist with synchronous vortices (see upper panels of figure 3(d)). As the external field increases, a proliferation of laggard vortices is observed with increasing velocity of dynamic pinning potential so that the maximum induced voltage tends to decrease. In this case, the peaks occur when the voltage increment produced by the synchronous vortices is equal to the voltage decrement caused by the laggard vortices. The lower panel of figure 3(d) shows that at high sliding velocity all vortices slip out from the dragging potential and arrange themselves forming dynamic vortex chains in the fast pinning potential channels (see supplemental movies for figures 3(c)–(e)[8]). With further increasing magnetic field, as shown in figure 3(e), the interstitial vortices can be observed between dynamic vortex chains. The interstitial vortices can move together with the dragged vortices at very low velocity. With increasing velocity, however, such interstitial vortices move quite slowly, and do not contribute significantly to V_y. As a consequence, one cannot expect to obtain a higher induced voltage by simply increasing magnetic field. A similar velocity dependence caused by shearing stress has been reported for an individual particle dragged through an assembly of other particles in the presence of quenched disorder [45].

3.2. Vortex drag across the lateral edges of the superconducting strip

Unlike the vortex dynamics along the x-axis discussed above, for $\theta = 90°$ the edge barrier will strongly affect the vortex dynamics. As a consequence, the resulting induced voltage characteristics $V_x(v_p)$ exhibit pronounced differences with respect to $V_y(v_p)$ as evidenced by comparing figures 4(a) with 3(a). The following two interesting features can be observed in the V_x curves at different magnetic fields. (i) The induced voltage V_x collapses rapidly to zero at high v_p because the pinning potential fails to couple to the vortices and drive them across the sample due to the presence of edge barriers. Notwithstanding the zero time-integrated voltage, the vortices do not remain static in this case and oscillate in the dynamic pinning channels, which yields an AC voltage signal. (ii) The induced voltage decreases in a stepwise fashion to zero, with the steps corresponding to well defined rates dV_x/dv_p. This phenomenon is reminiscent of the stroboscopic resonances between the vortex motion under applied current and the frequency of the time-varying dynamic pinning [33, 34]. At each step, V_x is proportional to v_p until it jumps down abruptly to another step. As a matter of fact, each characteristic slope of the steps (the dashed lines) can be linked to the ratio (n_s) of the number of vortices dragged into the sample to the number of the sliding pinning potential crossing the sample. One can see that n_s decreases with increasing v_p. At the first step, $n_s = 1$, and every pinning potential can drag vortices into the sample (figure 4(b)). At step of $n_s = 1/2$, alternating effective/ineffective rows of the pinning potential enter across the entry edge (bottom edge in the figure) with/without dragging vortices into the sample. For example, after a row of pinning sites drags vortices into the sample (see upper panel of of figure 4(c)), these vortices get detached from the dragging potential making the next coming row of the pinning potential ineffective due to the strong vortex-vortex interlocking (see lower panel of figure 4(c)). As a result, whether the vortices can nucleate at the entry edge and then dragged into and across the sample depends on the position of vortices inside the sample. The increasing rate of the induced voltage is determined by the coordinated movement of dynamic pinning potential with inner vortices. Eventually, the critical velocity at which the voltage V_x collapses to zero at various magnetic fields depends on the strength of edge barrier. The time evolutions of the induced voltage V_x and the animated data of the vortex dynamics are shown in supplemental figures (see footnote 7) and supplemental movies (see footnote 8), respectively.

It is worth noting that such stepwise behavior was not observed in the Giaever's system [5–7], since the width of the sample there was much larger than in the present sample. Figures 3 and 4 show that the velocity dependence of the induced voltage can be tuned by varying magnetic field in both cases of $\theta = 0°$ and 90°. This is more clearly observed in figure 5 where contour plots of the induced voltages V_y and V_x are presented as a function of the magnetic field and the velocity of dynamic pinning potential. In the case of $\theta = 0°$, high voltage can be observed in the red region with $0.42 < H_a < 0.58$ and $0.015 < v_p < 0.042$. The region of Meissner state in the case of $\theta = 0°$ (figure 5(a)) is slightly larger than that in the case of $\theta = 90°$ (figure 5(b)) because the vortex penetration field (related to the lower critical magnetic field H_{c1}) is decreased by the pinning potential sliding across the sample edge.

[7] See supplemental figures for the time evolutions of the induced voltages V_x and V_y (*i.e.* $V_x(t)$ and $V_y(t)$ curves) resulting from dragging vortices in the cases of $\theta = 0°$ and 90°.

[8] See supplemental movies for the vortex drag by the sliding pinning potential. Movies 1–2 for the upper and lower panels with low and high velocity of the dynamic pinning potential in figures 3(c)–(e). Movie 3 for figures 4(b)–(d).

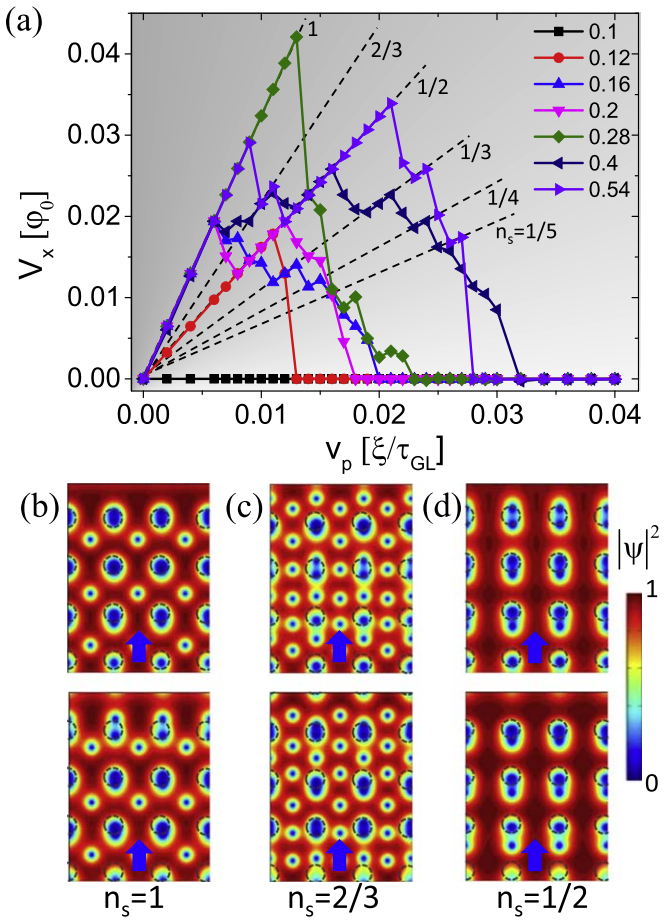

Figure 4. (a) The induced voltage (V_x) along the superconducting strip as a function of the velocity of the dynamic pinning potential v_p in the case of $\theta = 90°$ (i.e. when vortices are forced to cross the edge barrier) at different magnetic fields. The parameters of the dynamic pinnings are $R = 1.63$ and $a = 8.13$. (b)–(d) Snapshots of the Cooper-pair density corresponding to different increasing rate of voltage (n_s) by the sliding pinning potential with $v_p = 0.01$ (in units of ξ/τ_{GL}). (b) Every pinning site drags one vortex across the sample ($n_s = 1$) at $H_a = 0.28$; (c) $n_s = 2/3$ at $H_a = 0.4$ and (d) $n_s = 1/2$ at $H_a = 0.2$. Upper and lower panels are vortex states obtained with same parameters, but at different times. The strip has periodic boundary conditions along the horizontal direction. The time evolutions of the induced voltage V_x and the animated data of the dynamic vortex states can be seen in supplemental figures and movies (see footnotes 7 and 8).

3.3. Influence of parameters of the dynamic pinning sites

It is well known that the size and the density of static antidots or blind holes have a strong impact on the vortex pinning strength and resulting vortex configurations [44, 46–48]. Similar results should also be observed in the system with dynamic pinning potential. The vortex configurations for pinning size $R = 1.22, 2.03, 2.44$ in figure 6(a) show that each pinning potential can trap a giant vortex with vorticity 2, but the maximal vorticity of each site increases with increasing pinning size. Figures 6(b), (c) present the vortex states with varying density of the pinning potential at $H_a = 0.22$ and 0.34, respectively. The simulated areas vary according to the pinning density since we always choose three columns of pinning sites within the simulated region of the sample. Notwithstanding, this does not affect the results because of the periodic boundary conditions used in the x directions.

As anticipated, figures 7(a), (b) show that the pinning size has a strong impact on the induced voltage in both cases of $\theta = 0°$ and $\theta = 90°$. Although the same initial response of voltage V_x is obtained by sliding pinning potential of any size, V_x starts to decrease at lower velocity as pinning sites are made smaller. This indicates that the laggard vortices appear earlier with small size of pinning sites because of their weaker dragging ability. For the case of $\theta = 90°$, each pinning site with $R = 2.03$ and 2.44 can drag a giant vortex at low velocity, which results in a regime with $n_s = 2$ observed in figure 7(b). Figures 8(a), (b) show the induced voltage as a function of the velocity for different densities of the sliding pinning potential, moving along the superconducting strip and perpendicular to the edges, respectively. For the case of $\theta = 90°$, the different increasing rates (stepwise behavior) of voltage V_x by varying periods (a) depend on the number of the columns of the pinning sites in the simulated regime of width w. Figures 7–8 imply that the induced voltages V_y and V_x are increased significantly

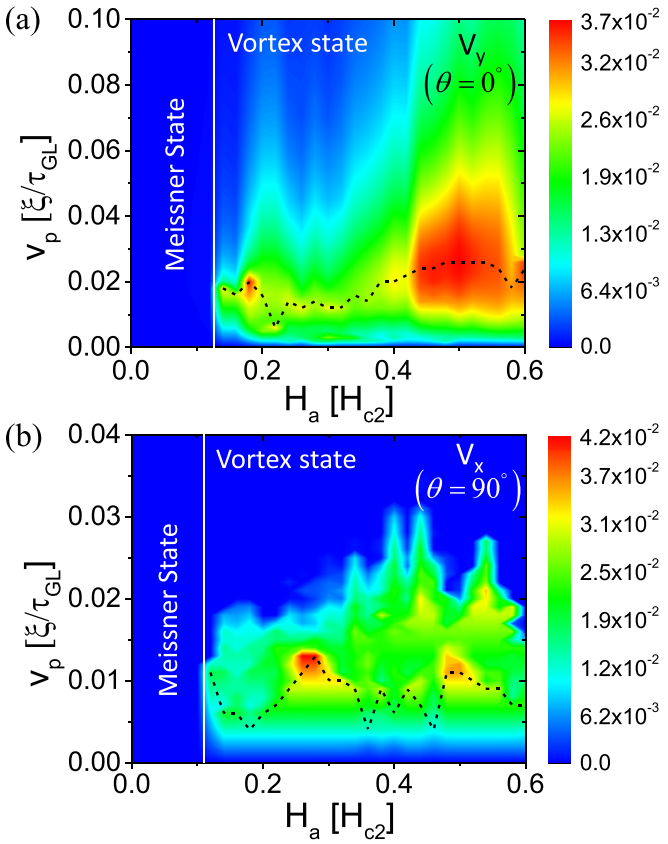

Figure 5. Contour plot of induced voltage V_y (a) and V_x (b) as a function of magnetic field H_a and velocity of dynamic pinning potential v_p. Dashed curves indicate v_p at the voltage peak at different magnetic fields.

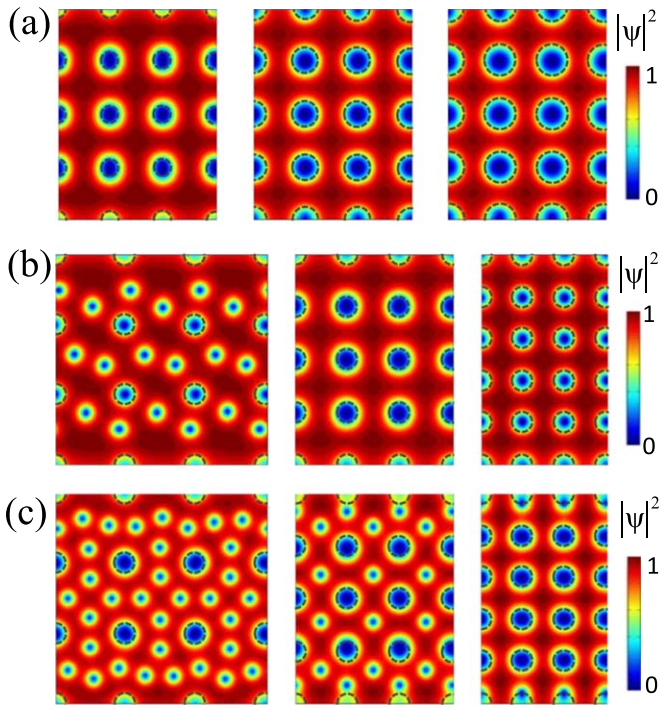

Figure 6. (a) Cooper-pair density snapshots showing the vortex states with static pinning potential ($a = 8.13$) at a magnetic field $H_a = 0.22$. The length of the simulated area is $L = 24.4$ and the sizes of the pinning sites (from left to right) are $R = 1.22$, 2.03 and 2.44. (b), (c) vortex states with different density of static pinning potential ($a = 10.84$, 8.13, and 6.50, with lengths of simulated area $L = 32.5$, 24.4 and 19.5, left to right respectively), at magnetic fields $H_a = 0.22$ (b) and 0.34 (c). The size of pinning sites is $R = 1.63$.

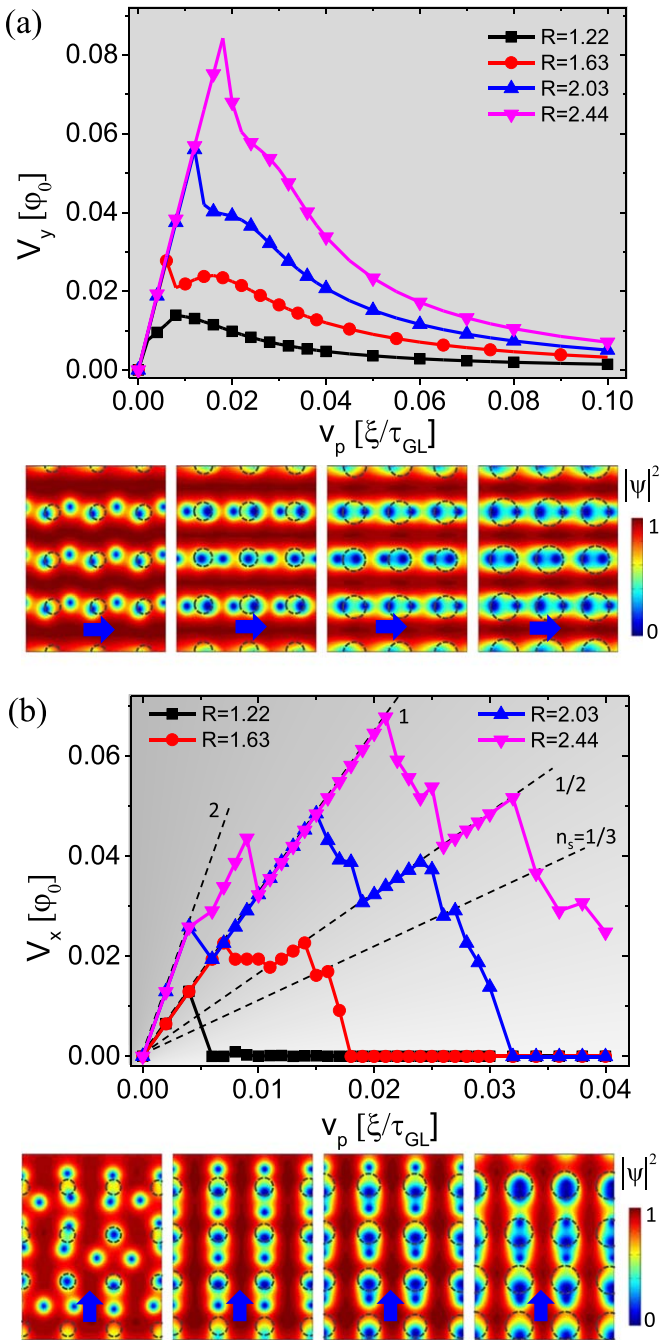

Figure 7. The velocity dependence of the induced voltages V_y (a) and V_x (b) for different sizes of dynamic pinnings ($R = 1.22, 1.63, 2.03$, and 2.44) at magnetic field $H_a = 0.22$ in the cases of $\theta = 0°$ and $\theta = 90°$. The period of pinning sites is $a = 8.13$, and the strip is along horizontal direction. The lower panels show the Cooper-pair density snapshots of the vortex dynamics with the velocity of the dynamic pinning potential $v_p = 0.04$ (a) and $v_p = 0.02$ (b), at $H_a = 0.22$.

when enhancing the dragging ability by increasing the size of pinning sites, or dragging more vortices in unit time by increasing the density of pinning sites and sample size.

Let us now discuss the vortex motion and induced voltages when tilting the sliding angle of the pinning potential. Figures 9(a), (b) present the induced voltages for the cases of $\theta = 30°, 45°$ and $60°$. One can see that V_y and V_x are both affected by edge barriers, simultaneously. It is important to point out that the superposition principle of the voltage by separately considering the components of velocity does not hold in this case. This becomes apparent when looking at the voltage V_x, where the stepwise features also appear in V_y at low velocity and low magnetic fields. Additionally, one can see that V_y decreases rapidly at high sliding velocity in $\theta = 30°$ and $60°$, which is similar to the case of $\theta = 0°$. However, such decreasing characteristics can be observed in V_y only at high magnetic fields in the case of $\theta = 45°$. At lower magnetic fields, it is striking to note that the voltage V_y collapses rapidly to zero at high sliding velocity, which is similar to the feature of V_x. As shown in the left panel of figure 9(c), tilted vortex chains consisting of static vortices can always be observed in the channels of the

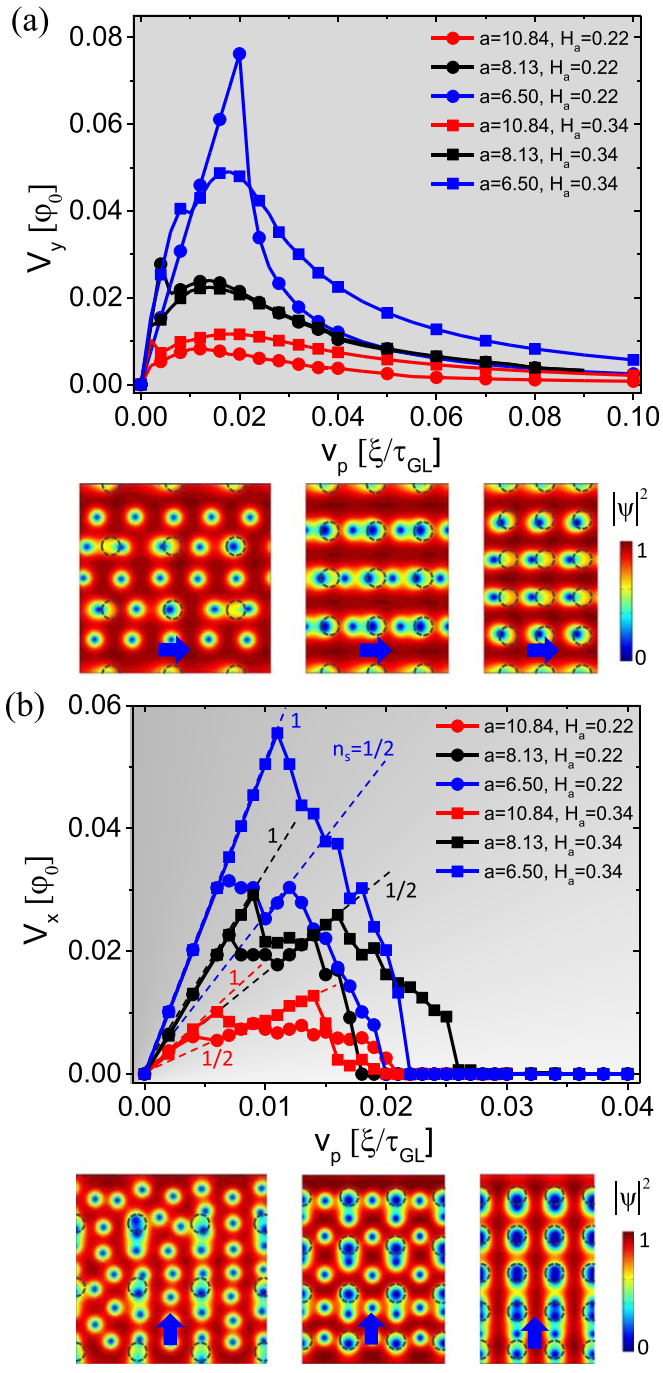

Figure 8. The velocity dependence of the induced voltages V_y (a) and V_x (b) for different density of dynamic pinning potential ($a = 10.84, 8.13$ and 6.50) at magnetic field $H_a = 0.22$ and 0.34, in the cases of $\theta = 0°$ and $\theta = 90°$. Presented snapshots show the Cooper-pair density of vortex motion for different densities of dynamic pinning potential, for $v_p = 0.03$ and $H_a = 0.22$ (a), and $v_p = 0.015$ and $H_a = 0.34$ (b). The strip is along the horizontal direction.

dynamic pinning potential due to the interlocking effect of the vortex lattice and the edge barriers. Nevertheless, the interlocking effect is broken easily by the interstitial vortices at higher magnetic fields (see right panel of figure 9(c)) so that V_y can still be observed. Furthermore, as shown in the left panel of figure 9(d), the vortices can arrange themselves forming vortex chains, in this case with tilt angle of 64°, which does not exactly match the channels of the dynamic pinning potential (60°). Therefore, unlike the case of $\theta = 45°$, the driving force of the dynamic pinning potential yields a component of velocity along x-axis, such that V_y can still be observed for $\theta = 30°$ and 60°.

Thus far, we have discussed the open circuit voltage generated by a sliding pinning potential landscape. This system represents a mesoscopic planar dynamo able to convert mechanical energy into electricity. When loaded with a resistance, a current would circulate in the circuit and enhance the damping of the vortex motion. As a

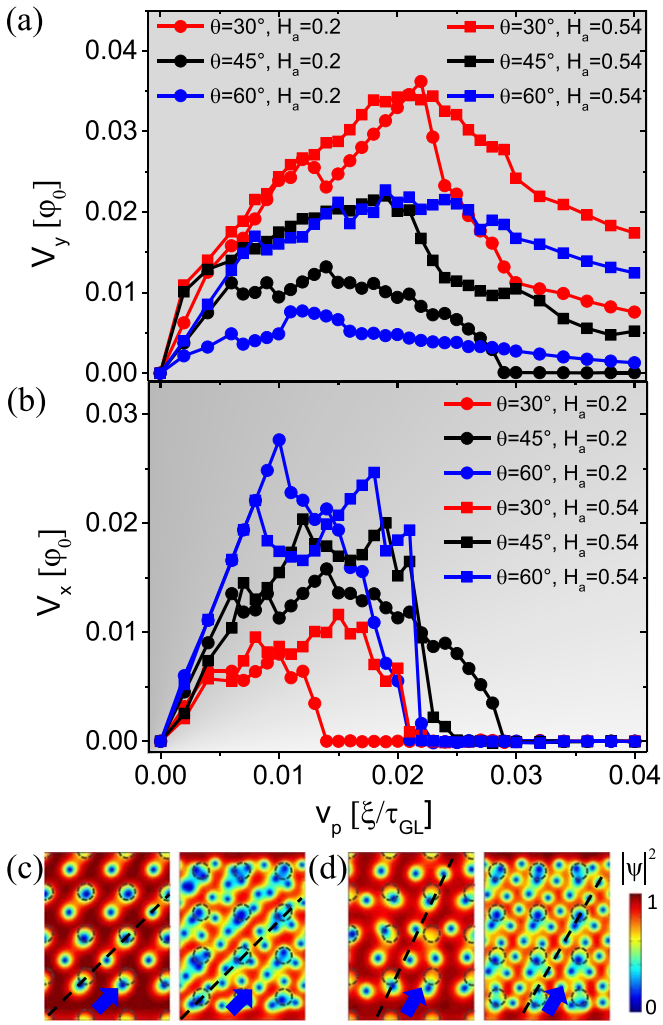

Figure 9. (a), (b) The induced voltage V_y (a) and V_x (b) as a function of the velocity of the dynamic pinning potential along a tilted angle $\theta = 30°, 45°$ and $60°$, at different magnetic fields. (c), (d) The vortex states with the sliding pinning potential (for $v_p = 0.03$) with the tilt angle $\theta = 45°$ (c) and $60°$ (d), at magnetic field $H_a = 0.2$ (left panels) and 0.54 (right panels). Blue arrows and black dashed lines in panels (c) and (d) show the dragging direction of the pinning potential and the resulting tilt angle of the vortex chains, 45°, 45°, 64° and 60° (respectively from left to right).

consequence, the decoupling transition between synchronous and laggard vortices would shift to lower v_p values.

4. Conclusions

In summary, we analyzed a mesoscopic planar dynamo effect realized by dragging vortices with a dynamic pinning potential in a superconducting strip. Based on the Ginzburg–Landau simulations, we find that the open circuit voltage resulting from the coexisting synchronous/laggard vortices and the dynamic vortex chains, can be tuned by varying the velocity of the sliding pinning potential and/or by varying the magnetic field. The edge barriers have a strong impact on the induced voltage and the vortex dynamics. In particular, significantly different characteristics of the induced voltage are observed in the cases of dragging the vortices along the superconducting strip or perpendicular to the sample edges. This work conceptually extends Giavers's dc transformer device by including arbitrary in-plane dragging directions and a tunable mismatch between the vortex density and the pinning site density. The vortex drag and the resulting induced voltage can be tuned by the size, density and the sliding direction of the pinning potential. The results of this work therefore provide new insights into possible spatio-temporal vortex manipulations, employable in further fundamental and technological advances of hybrid superconducting systems. Furthermore, the growing interest in manipulation of vortices in the iron-chalcogenides and the Majorana zero modes in their cores [49–51], might position targeted dragging of vortices as an appealing approach towards quantum operations with Majorana fermions.

Acknowledgments

CX and AH acknowledge support by the National Natural Science Foundation of China (Grant Nos. 11972298, 11702218 and 11702034), Natural Science Basic Research Plan in Shaanxi Province of China (Grant Nos. 2018JM1003, 2018JQ1074), Young Talent Fund of University Association for Science and Technology in Shaanxi, China (Grant Nos. 20180501, 20180503), and the Fundamental Research Funds for the Central Universities (Grant Nos. 300102129104, 3102018zy013, and 3102017jc01003). MVM acknowledges support from the Research Foundation—Flanders (FWO) and the special research funds (BOF) of the University of Antwerp, Belgium. The collaborative effort in this work was fostered by the EU-COST Action CA16218 NANOCOHYBRI.

ORCID iDs

Cun Xue https://orcid.org/0000-0001-6255-2837
Milorad V Milošević https://orcid.org/0000-0002-5431-377X
Alejandro V Silhanek https://orcid.org/0000-0001-9551-5717

References

[1] Grinberg A A 1970 *Zh. Eksp. Teor. Fiz.* **58** 989
Grinberg A A 1970 *Sov. Phys.—JETP* **31** 531
[2] Gibson A F, Kimmitt M F and Walker A C 1970 *Appl. Phys. Lett.* **17** 75
[3] Gibson A F and Walker A C 1971 *J. Phys. C: Solid State Phys.* **8** 2209
[4] Cameron K, Gibson A F, Giles J, Hatch C B, Kimmitt M F and Shafik S 1975 *J. Phys. C: Solid State Phys.* **8** 3137
[5] Giaever I 1965 *Phys. Rev. Lett.* **15** 825
Giaever I 1966 *Phys. Rev. Lett.* **16** 460
[6] Solomon P R 1966 *Phys. Rev. Lett.* **16** 50
[7] Ekin J W, Serin B and Clem J R 1974 *Phys. Rev.* B **9** 912
[8] Bumby C W, Jiang Z, Storey J G, Pantoja A E and Badcock R A 2016 *Appl. Phys. Lett.* **108** 122601
[9] Danckwerts M, Goñi A R, Thomsen C, Eberl K and Rojo A G 2000 *Phys. Rev. Lett.* **84** 3702
[10] Gramila T J, Eisenstein J P, MacDonald A H, Pfeiffer L N and West K W 1991 *Phys. Rev. Lett.* **66** 1216
[11] Rojo A G 1999 *J. Phys.: Condens. Matter* **11** R31
[12] Tung S, Schweikhard V and Cornell E A 2006 *Phys. Rev. Lett.* **97** 240402
[13] Reichhardt C, Bairnsfather C and Olson Reichhardt C J 2011 *Phys. Rev.* E **83** 061404
[14] Olson Reichhardt C J and Reichhardt C 2008 *Phys. Rev.* E **78** 011402
[15] Straver E W J, Hoffman J E, Auslaender O M, Rugar D and Moler K A 2008 *Appl. Phys. Lett.* **93** 172514
[16] Auslaender O M, Luan L, Straver E W J, Hoffman J E, Koshnick N C, Zeldov E, Douglas A B, Liang R X, Hardy W N and Moler K A 2008 *Nat. Phys.* **5** 35
[17] Ma X, Reichhardt C J O and Reichhardt C 2018 *Phys. Rev.* B **97** 214521
[18] Gardner B W, Wynn J C, Bonn D A, Liang R X, Hardy W N, Kirtley J R, Kogan V G and Moler K A 2002 *Appl. Phys. Lett.* **80** 1010
[19] Kalisky B, Kirtley J R, Analytis J G, Chu J-H, Fisher I R and Moler K A 2011 *Phys. Rev.* B **83** 064511
[20] Kremen A, Wissberg S, Haham N, Persky E, Frenkel Y and Kalisky B 2016 *Nano Lett.* **16** 1626
[21] Veshchunov I S, Magrini W, Mironov S V, Godin A G, Trebbia J-B, Buzdin A I, Tamarat P and Lounis B 2016 *Nat. Commun.* **7** 12801
[22] Ge J-Y, Gladilin V N, Tempere J, Xue C, Devreese J T, Van de Vondel J, Zhou Y-H and Moshchalkov V V 2017 *Nat. Commun.* **7** 13880
[23] Aladyshkin A Y, Silhanek A V, Gillijns W and Moshchalkov V V 2009 *Supercond. Sci. Technol.* **22** 053001
[24] Kramer R B G, Silhanek A V, Gillijns W and Moshchalkov V V 2011 *Phys. Rev.* X **1** 021004
[25] Rodrigo P J, Eriksen R L, Daria V R and Glückstad J 2002 *Opt. Express* **10** 26
[26] Brunner M and Bechinger C 2002 *Phys. Rev. Lett.* **88** 248302
[27] Grier D G 2003 *Nature* **424** 810
[28] Lee S H, Ladavac K, Polin M and Grier D G 2005 *Phys. Rev. Lett.* **94** 110601
[29] Libál A, Reichhardt C, Jankó B and Olson Reichhardt C J 2006 *Phys. Rev. Lett.* **96** 188301
[30] Roichman Y, Wong V and Grier D G 2007 *Phys. Rev.* E **75** 011407
[31] Righini M, Zelenina A S, Girard C and Quidant R 2007 *Nat. Phys.* **3** 477
[32] Dahir S M, Volkov A F and Eremin I M 2019 *Phys. Rev. Lett.* **122** 097001
[33] Jelić Ž L, Milošević M V, Van de Vondel J and Silhanek A V 2015 *Sci. Rep.* **5** 14604
[34] Jelić Ž L, Milošević M V and Silhanek A V 2016 *Sci. Rep.* **6** 35687
[35] Kramer L and Watts-Tobin R J 1978 *Phys. Rev. Lett.* **40** 1041
[36] Vodolazov D Y and Peeters F M 2007 *Phys. Rev.* B **76** 014522
[37] Watts-Tobin R J, Krähenbühl Y and Kramer L 1981 *J. Low Temp. Phys.* **42** 459
[38] Berdiyorov G R, Milošević M V and Peeters F M 2009 *Phys. Rev.* B **79** 184506
[39] Berdiyorov G R, Milošević M V, Latimer M L, Xiao Z L, Kwok W K and Peeters F M 2012 *Phys. Rev. Lett.* **109** 057004
[40] Gropp W D, Kaper H G, Leaf G K, Levine D M, Palumbo M and Vinokur V M 1996 *J. Comput. Phys.* **123** 254
[41] Lombardo J, Jelić Ž L, Baumans X D A, Scheerder J E, Nacenta J P, Moshchalkov V V, Van de Vondel J, Kramer R B G, Milošević M V and Silhanek A V 2018 *Nanoscale* **10** 1987
[42] Adami O-A, Jelić Ž L, Xue C, Abdel-Hafiez M, Hackens B, Moshchalkov V V, Milošević M V, Van de Vondel J and Silhanek A V 2015 *Phys. Rev.* B **92** 134506
[43] Kramer R B G, Ataklti G W, Moshchalkov V V and Silhanek A V 2010 *Phys. Rev.* B **81** 144508
[44] Moshchalkov V, Woerdenweber R and Lang W 2010 *Nanoscience and Engineering in Superconductivity* (Berlin: Springer)

[45] Libál A, Csíki B M, Olson Reichhardt C J and Reichhardt C 2013 *Phys. Rev.* E **87** 022308
[46] Ray D, Olson Reichhardt C J, Jankó B and Reichhardt C 2013 *Phys. Rev. Lett.* **110** 267001
[47] Wang Y L, Latimer M L, Xiao Z L, Divan R, Ocola L E, Crabtree G W and Kwok W K 2013 *Phys. Rev.* B **87** 220501(R)
Wang Y L, Thoutam L R, Xiao Z L, Shen B, Pearson J E, Divan R, Ocola L E, Crabtree G W and Kwok W K 2016 *Phys. Rev.* B **93** 045111
[48] Berdiyorov G R, Milošević M V and Peeters F M 2009 *New J. Phys.* **11** 013025
[49] Posske T, Chiu C-K and Thorwart M 2019 arXiv:1908.03576
[50] November B H, Sau J D, Williams J R and Hoffman J E 2019 arXiv:1905.09792
[51] Beenakker C W J, Baireuther P, Herasymenko Y, Adagideli I, Lin Wang and Akhmerov A R 2019 *Phys. Rev. Lett.* **122** 146803